Separation and Purification Technology 203 (2018) 209–216

Contents lists available at ScienceDirect

Separation and Purification Technology

journal homepage: www.elsevier.com/locate/seppur

Engineering cellulose fibre inorganic composites for depth filtration and adsorption

Aysu Onur[a], Aaron Ng[b], Gil Garnier[a,*], Warren Batchelor[a,*]

[a] BioProcessing Research Institute of Australia (BioPRIA), Chemical Engineering Department, Monash University, Clayton, Australia
[b] 3M Australia, Sydney, Australia

ARTICLE INFO

Keywords:
Depth filter
Adsorption
Filtration
Cellulose nanofibre
Composite

ABSTRACT

Depth type composite filters are porous materials heavily loaded with adsorbents and can remove contaminants from liquids by combining mechanical entrapment and adsorption. There is still a need for developing high performance filters by controlling the internal structure at micro and nano level. In this study, highly fibrillated nanocellulose (NC) with increased surface area was used as partial substitute for the fibre matrix to tailor the filter structure as well as the adsorption and filtration performance. Polyamide-amine-epichlorohydrin (PAE) was added both to adjust the charge of medium and provide wet strength. Filters were fabricated by embedding perlite particles into the cellulose fibre matrix by papermaking technique. The structure of composites was characterized for pore size distribution and surface morphology. Adsorption and filtration characteristics were quantified using two model dyes and silicon dioxide particles. Adsorption was found to be electrostatically controlled and dependent on the charge of the dye molecules and the filter medium. The addition of NC doubled the removal of a cationic dye by increasing the surface area and the available negative charges; it however decreased the removal of an anionic dye by 75%. PAE addition decreased the adsorption of the cationic methylene blue dye, while increasing the adsorption of the anionic metanil yellow dye. Rejection by filtration of 1 µm particles was over 90% for all filters. This study demonstrates that highly fibrillated NC fibres combined with a cationic wet strength polyelectrolyte can be used to tailor the filter structure and properties.

1. Introduction

Liquid filtration is used in a vast range of applications such as water treatment, beverage and juice filtration, pharmaceutical and industrial chemical filtration as well as medical purposes such as blood filtration [1]. Membrane technology plays an important role in liquid filtration applications and polymeric membranes made of polyamide, polysulfone and polyimide are widely used [2] due to their mechanical and chemical resistances. However, these membranes suffer environmental drawbacks as they are petroleum based, non-biodegradable and large quantities of solvents and chemicals [3] are required for their production. These membranes perform separation only by filtration/size exclusion and remain inefficient for the separation of small charged molecules. In addition, membrane technology mainly relies on separation at the surface which is very susceptible to fouling [4]. There is a need for environmentally benign products with improved functionalities that can be reprocessed, recycled or will biodegrade at the end of their life. Depth type composites using cellulose fibres provide a solution. Depth filters are porous materials heavily loaded with adsorbents. These filters retain molecules not only on the surface but also within the media [5]. They can remove contaminants from liquids by combining filtration/mechanical entrapment with adsorption, resulting in a higher removal capacity.

Nanocellulose (NC) has widely been explored as an alternative polymer in membranes/filters due to unique properties such as high surface area, high strength, wettability, ease of chemical functionalization and low environmental impact [6]. Cellulose is the most abundant polymer and can be used in the form of fibres and derivatives in a vast range of products [7–10]. NC technology has significantly progressed in the last decade; the applications of NC were reviewed by Salas et al. [11]. The potential of NC in filtration applications and its excellent adsorption capacity due to its high surface area-to-volume ratio have long been identified [12–18]. Even though NC performance for water treatment was demonstrated, most studies have focused on functionalized NC fibres with a variety of chemistries, improving pollutants binding efficiency [13,19,20]. This functionalization often requires expensive and toxic chemical treatments and can be difficult to scale up, limiting industrial applications. Also, regulations for some

* Corresponding authors at: BioProcessing Research Institute of Australia (BioPRIA), Chemical Engineering Department, Monash University, 3800, Australia.
E-mail addresses: gil.garnier@monash.edu (G. Garnier), warren.batchelor@monash.edu (W. Batchelor).

https://doi.org/10.1016/j.seppur.2018.04.038
Received 13 December 2017; Received in revised form 12 April 2018; Accepted 15 April 2018
Available online 17 April 2018
1383-5866/

applications, such as food and beverage, often restrict filters' chemical modification. The filters should be as chemical modification free as possible.

Some studies have quantified adsorption with NC based adsorbents using static experiments [13,16,18]; however, very few have reported particle rejection with dynamic experiments [14,15]. This is unfortunate as industry typically operates filters in a continuous mode instead of in a batch mode. NC composites with nano-ranged pore sizes have been explored for separation applications [21]. Keshavarzi et al. [22] investigated odour elimination with NC-zeolite composites in separation processes. However, limited number of studies have quantified NC composite performance in liquid filtration/adsorption. The following section gives an overview of dynamic studies of liquid filtration or adsorption with NC composites.

Varanasi et al. [23] reported the preparation of NC composite membranes and showed their potential in ultrafiltration. Silica nanoparticles were used to control the pore size of the nanofiber network. The pure NC membranes had high flux but the rejection of polyethylene glycol (PEG) was low because of the large pores. Composite membranes showed better rejection performance as the pore size was controlled by the silica nanoparticles. Control of composite pore size by nano particles addition is a promising avenue in ultrafiltration. However, this study focused on molecular weight cut off (MWCO) and ignored composite adsorption capability.

Karim et al. [24] investigated cellulose nano composites with functional cellulose nanocrystals added on a supporting layer of microsized cellulose fibres for adsorbing heavy metal ions from waste water. Nanocrystals promoted adsorption and the membranes showed excellent removal of metal ions. However, filtration was ignored and the isolation of cellulose nanocrystals from cellulose sludge is a tedious process requiring chemical treatment.

There is a lack of fundamental separation understanding in terms of combining adsorption and size exclusion for NC fibre composites under dynamic conditions. However, separation combining both adsorption and size exclusion is needed for some applications. In beer and wine filtration, for instance, it is necessary to remove bacteria and yeast particles to eliminate haziness [25] as well as removing some ionic compounds to avoid bitter taste [26–28].

This study aims developing microporous filters with mechanically-treated NC fibres and perlite, a low cost inorganic adsorbent. Composite filters combining adsorption and filtration are prepared with a simple and scalable papermaking process. The performance of highly fibrillated NC as a partial substitute for the fibre matrix of the filters is studied. Polyamide-amine-epichlorohydrin (PAE), a cationic and cross-linking polyelectrolyte was selected to provide wet strength and control the charge of the medium; PAE is food grade when fully crosslinked. Filtration and adsorption performances are evaluated dynamically with two model dyes and silicon dioxide particles and analysed in the context of food and pharmaceutical applications.

2. Materials and methods

2.1. Materials

The cellulose fibres used for the composites are unrefined northern softwood NIST RM 8495 bleached kraft pulp (with a typical fibre length of around 2.5–4 mm and 30 µm wide) and bleached radiata pine softwood kraft pulp refined to 400 Canadian standard freeness (CSF) in a disk refiner. Highly fibrillated NC fibres were prepared by processing refined pulp in a GEA Niro Soavi homogenizer at 800 bar at both 1 pass and 3 passes.

Expanded perlite supplied by Dicalite Minerals Corp was used as an inorganic adsorbent. Commercial PAE provided from Nopcobond Paper Technology Pty Ltd was used as wet strength resin.

Methylene blue (MB) and metanil yellow (MY) dyes supplied from Sigma Aldrich were used to test adsorption. 1 µm monodisperse silicon dioxide particles from Sigma Aldrich were used to test filtration capability of the composites.

2.2. Methods

2.2.1. Preparation of filters

Prior to sheet preparation, dry pulp was soaked in 2 L deionised water overnight and then disintegrated by a model MKIIIC, Messmer Instruments Ltd for 75,000 revolutions. Following disintegration, sheet suspensions were prepared by adding perlite suspensions to the pulp suspensions. PAE (0.22% w/v) was then added at a rate of 100 mg/g fibre and the mixtures were hand mixed before sheet making. 5 different composites and a control cellulose sheet were prepared; the fibre component was varied as described with only 1/3 of the cellulose fibre component. Composites were labelled based on the fibre composition and presence of perlite and polymer as follow:

(1) **Refined** – 100% Fibre (1/3 refined pulp + 2/3 unrefined pulp)
(2) **Refined/Per/PAE** – 30% Fibre (1/3 refined pulp + 2/3 unrefined pulp) + 70% Perlite + 120 mg PAE
(3) **Unrefined/Per/PAE** – 30% Fibre (3/3 unrefined pulp) + 70% Perlite + 120 mg PAE
(4) **Homogenized(1pass)/Per/PAE** – 30% Fibre (1/3 homogenized (1 pass) + 2/3 unrefined pulp) + 70% Perlite + 120 mg PAE
(5) **Homogenized(3pass)/Per/PAE** – 30% Fibre (1/3 homogenized (3 pass) + 2/3 unrefined pulp) + 70% Perlite + 120 mg PAE
(6) **Homogenized(3pass)/Per** – 30% Fibre (1/3 homogenized (3 pass) + 2/3 unrefined pulp) + 70% Perlite

The cellulose component was always kept constant at 60 g per square metre (gsm). For the composites with perlite, the target total gsm was 200 gsm- assuming full retention.

A British hand sheet maker was used to form the composite filters. A wet strengthened qualitative filter paper was deposited over the 150 µm size mesh and the suspension was poured into the chamber and then drained through the filter paper to form the sheets uniformly. After sheet formation, the wet sheet was separated from the mesh, placed between dry blotting papers and pressed under 345 kPa for 5 min. The composites containing PAE were heated 30 min at 105 °C for curing and then air-dried in a humidity room (23 °C, 50% relative humidity) overnight. The sheets without PAE were air-dried in the humidity room for at least 24 h without any oven treatment.

2.2.2. Mercury porosimetry

Composite pore size distribution was measured with a Micromeritics' AutoPore IV 9500 series. This technique quantifies a material's pore size distribution and porosity by applying increasing pressures (up to 60,000 psia) to a sample immersed in mercury and recording the volume of mercury intruded into pores. Samples were cut into approximately 5 mm × 5 mm small pieces and degassed for at least two days prior to characterization. A penetrometer with 0.412 mL stem volume was used to carry out the measurements. After degassing, approximately 0.1 g of sample was placed in the penetrometer and the analysis conducted. The volume of mercury intruded into pores is converted to equivalent pore sizes using the instrument software [29].

2.2.3. Scanning electron microscopy (SEM)

A FEI Nova NanoSEM 450 FEG SEM and a FEI Magellan 400 FEG SEM were used to characterize surface and bulk morphology of composites and estimate fibre diameter. Samples were mounted onto a metal substrate using carbon tape and coated with a thin layer of Iridium. Secondary electron images of composites were captured. 2 kV of accelerating voltage was applied for magnification up to 100,000. For fibre diameter measurement, silicon chips were used to cast the fibres and iridium coating was applied.

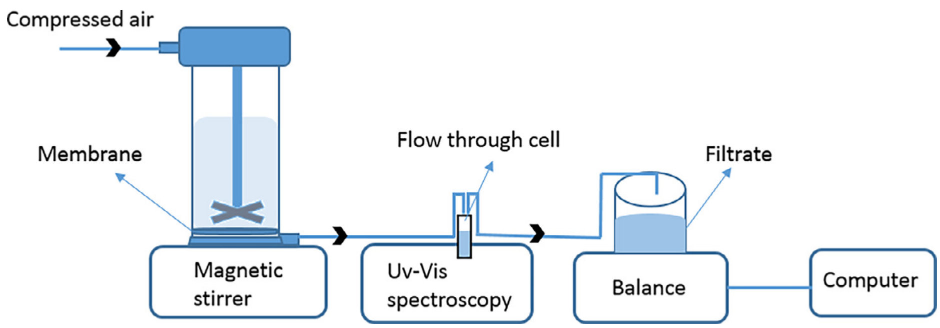

Fig. 1. Schematic illustration of the stirred cell experimental setup.

2.2.4. Adsorption and filtration

A Merck Millipore, model UFSC40001 dead-end stirred cell was used for adsorption and filtration experiments. The stirred cell is pressure driven with a 0.00418 m^2 effective membrane area and 400 mL working volume. Samples were placed on the membrane holder at the bottom and the cell body was filled with the prepared solution. The system was closed and pressurized by a compressed air gas cylinder. Filtrate was passed through a quartz micro flow cell with 10 mm optical path length sitting in an ultraviolet-visible (UV–vis) absorption spectrometer and transferred to a beaker on a balance. Both instantaneous absorbance and weight of the filtrate were measured every 10 s. The schematic system is illustrated in Fig. 1.

Preliminary adsorption experiments, performed at pressures ranging from 1 to 3 bar, identified the optimum inlet pressure as 1.5 bar; data is provided in the supplementary section (Fig. S1). Adsorption results were determined at 1.5 bar with 400 mL of 5 ppm dye solution. 5 ppm dye solutions were prepared by dissolving 5 mg of dye in 1 L deionized water. Breakthrough curves were obtained by plotting the instantaneous concentration (normalized by the initial concentration) as a function of time. The calibration curves are provided in supplementary information (SI) (Fig. S2). Dye removal was measured from the concentration of initial feed solution and filtrate:

$$Dye\ removal\,(\%) = \frac{\text{Initial dye concentration} - \text{filtrate dye concentration}}{\text{Initial dye concentration}} \times 100 \tag{1}$$

Adsorption capacity of each filter was calculated with the following equation. The integral was calculated from the area over the curve by trapeze method. Methylene blue and metanil yellow adsorption capacities of the filters were given in SI (Table SI and SII)

$$q = \frac{CF*Q}{1000*ms}\int\frac{1-Cout}{CF} \tag{2}$$

where:

q: Capacity of the adsorbent (mg/g)
C_{out}: Concentration of filtrate (mg/g)
C_F: Concentration of feed (mg/g)
Q: Volumetric flow rate (cm^3/s)
t: Time (s)
m_s: Weight of adsorbent (g)

Filtration efficiency was measured with a 0.05 wt% suspension of 1 µm silicon dioxide particles. Experiments were also conducted at 1.5 bar and concentration of silicon dioxide in suspension was measured before and after filtration by UV–vis spectroscopy to calculate filter rejection:

$$Rejection\,(\%) = \frac{\text{Initial feed concentration} - \text{Filtrate concentration}}{\text{Initial feed concentration}} \times 100 \tag{3}$$

Flux was calculated from the time to filter all of the suspension as:

$$FLUX\,(LMH) = \frac{Volume\ of\ filtrate\,(L)}{area\,(\text{m2}) \times time\,(h)} \tag{4}$$

Water was passed through the filters to remove any contaminants prior to adsorption and filtration experiments.

3. Results

3.1. Filter structure

3.1.1. Fibre size distribution

Fibre diameter size distribution of refined and homogenized pulps was measured from SEM images. High magnification images (Fig. 2) from completely different points of samples were acquired with at least 100 individual fibres in total and the diameter of every individual fibre in standard pictures was measured by image J, image processing software. The effect of increased fibrillation by mechanical treatment is seen on Fig. 2a–c. Low magnification images show that large fibres are still present even after homogenization (SI, Fig. S4). Histograms present fibre diameter size distributions estimated from the high magnification images in Fig. 3.

The majority of the refined fibres in the high magnification images have a diameter centred between 45 nm and 50 nm and the diameter is decreasing with the intensity of homogenization treatment. The average fibre diameters measured in these images fall to 25 to 40 nm after 1 pass and 20–25 nm after 3 passes homogenization.

Additionally, particle size distribution of perlite particles was measured by the same technique and can be found in SI (Fig S5).

3.1.2. Pore size distribution

Filter pore size distribution was measured by mercury porosimetry (Fig. 4). The distribution of pore size ranges from 1 to 3 µm. Substitution of fibre composition with homogenized pulp resulted in smaller pore sizes.

The cellulose sheet (*Refined*) has a smaller pore size distribution compared to composite combining refined pulp, perlite and PAE (*Refined/Per/PAE*) even though the fibre content is identical. Perlite addition increased the composite pore size by adsorbing between fibres. The peak intensity is also significantly smaller which reflects that the number of pores at a specific pore size is lower.

The slight difference between pore sizes of composites *Homogenized (3pass)/Per* and *Homogenized(3pass)/Per/PAE* demonstrates the effect of PAE addition. The sample with PAE (*Homogenized(3pass)/Per/PAE*) has a slightly smaller pore size.

3.1.3. Surface morphology

SEM images of filters made with different pulps homogenized to different intensities are shown in Fig. 5. Connectivity between fibres and perlite particles increases with the entangled network created by highly fibrillated NC addition (Fig. 5a–d). This connectivity results in a smoother, more closed surface and a decrease in composite porosity.

The arrows in Fig. 5 highlight the changes in surface morphology.

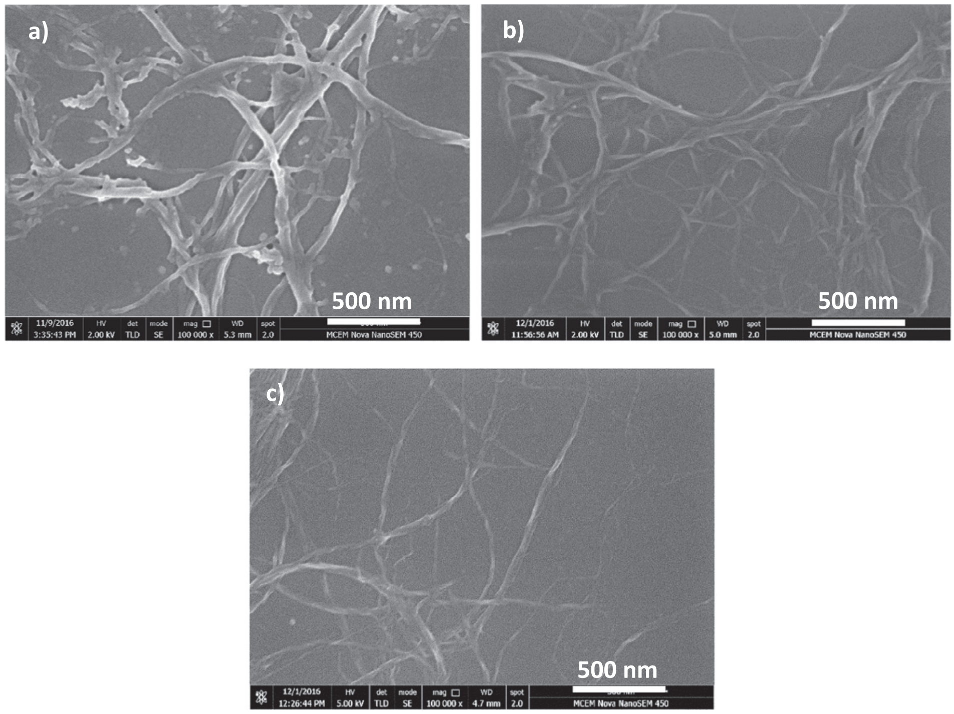

Fig. 2. High magnification SEM images of: **(a)** Refined pulp, **(b)** Homogenized pulp by 1 pass and **(c)** Homogenized pulp by 3 passes.

Arrows (i) and (ii) show the perlite particles with sharp edges which became blurred with homogenized pulp addition in arrows (iv). Addition of highly fibrillated NC smooths the edges and binds the perlite particles. Arrow (iii) shows the presence of some remaining large fibres in sample *Homogenized(1pass)/Per/PAE*.

3.2. Adsorption and filtration

3.2.1. Adsorption with breakthrough curves

The breakthrough curves measured at 1.5 bar for all samples with MY and MB dye solutions are shown in Fig. 6a and b, respectively. Breakthrough curves present the normalized concentrations as a function of time or effluent volume. They usually show a characteristic S shape with varying degrees of steepness. All outlet concentrations are presented normalized with the inlet concentration: C/Co ranges from 0, for full adsorption, to 1, for no adsorption. Initially, the dye molecules are adsorbed very effectively on the fresh adsorbent and the outlet concentration equals zero. As the filters start to saturate, the outlet concentration gradually approaches the inlet concentration and the normalized concentration (C/Co) increases to eventually level-off at

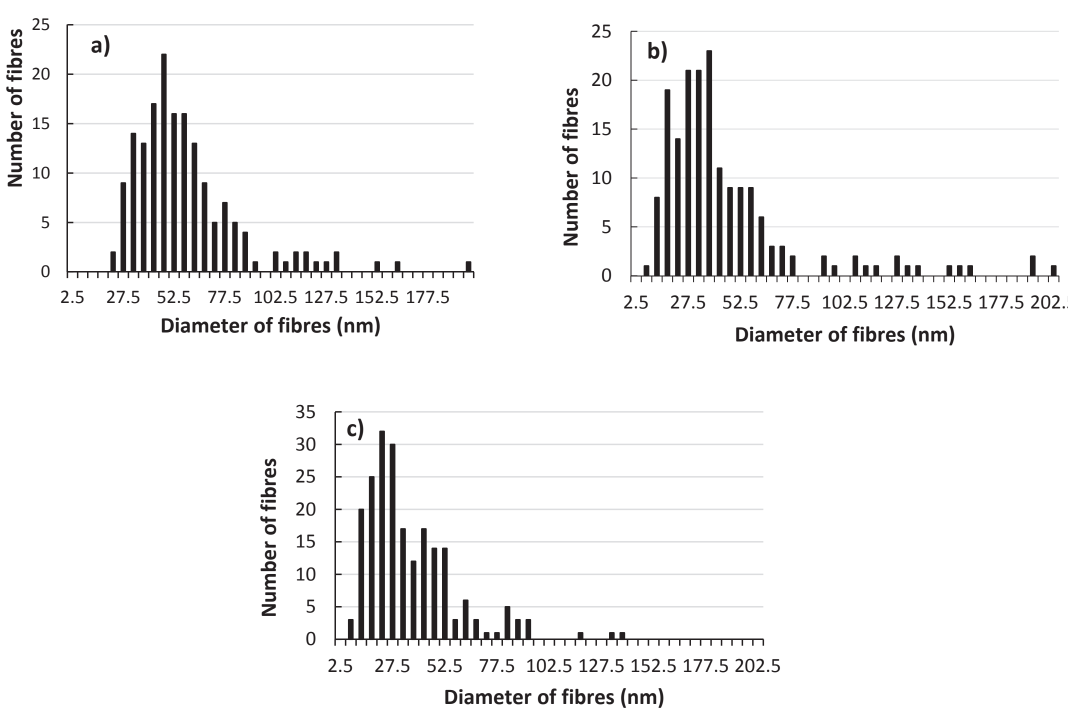

Fig. 3. Fibre size distribution of **(a)** Refined pulp **(b)** Homogenized pulp by 1 pass **(c)** Homogenized pulp by 3 passes.

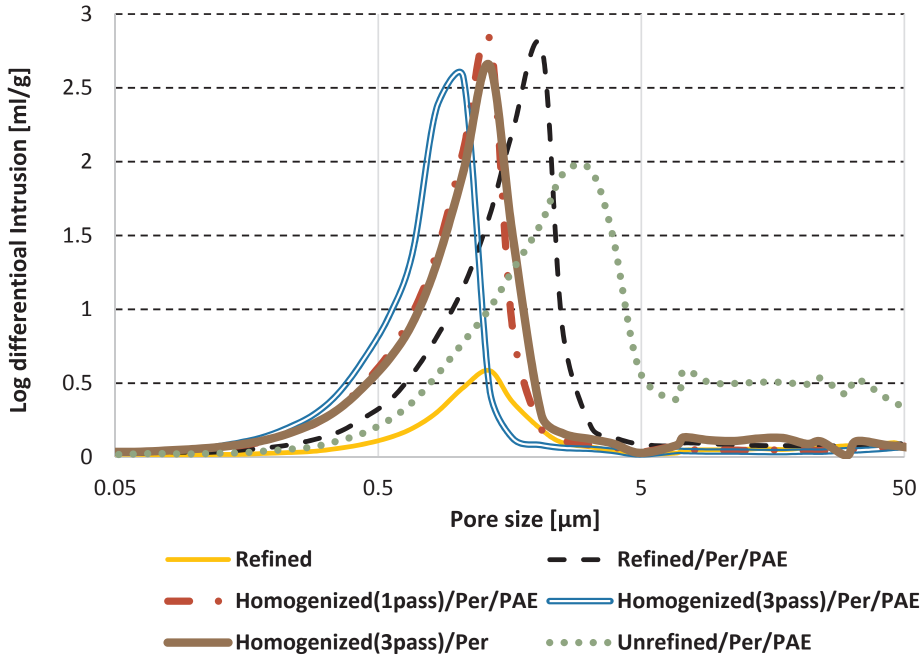

Fig. 4. Pore size distributions of filters measured by mercury porosimetry; effect of homogenization intensity and addition of perlite and PAE.

one.

The two oppositely charged dyes showed two opposite adsorption behaviours onto the composites (Fig. 6a and b). Basically no adsorption was recorded for the cationic MY dye onto cellulose sheet (*Refined*) or composite made with homogenized fibres (3 passes) with no PAE (*Homogenized(3pass)/Per*) (Fig. 6a). By contrast, the cationic MB showed some affinity and retention onto these same composites (Fig. 6b). Here, *Homogenized(3pass)/Per* presents the straightest breakthrough curve which indicates very strong attractive forces with MB- in the absence of positively charged PAE. The very intense blue colour of the saturated filter after adsorption (Fig. 6b) indicates more MB adsorbed onto the composite with highly fibrillated pulp content (*Homogenized(3pass)/Per*).

Adsorption occurs slightly differently for composites made only with refined pulp and those made with two different homogenized pulps treated at different intensities. As fibre fibrillation increases (homogenization or more passes in homogenization), composites increasingly repel the anionic dye- metanil yellow and attract the cationic dye (MB). From *Refined/Per/PAE* through *Homogenized(3pass)/Per/PAE* sample, attraction with MB (Fig. 6b) and repulsion with MY (Fig. 6a) increases with the fibrillation and increased surface area.

Flux and total dye removal were measured (Fig. 7). A maximum of

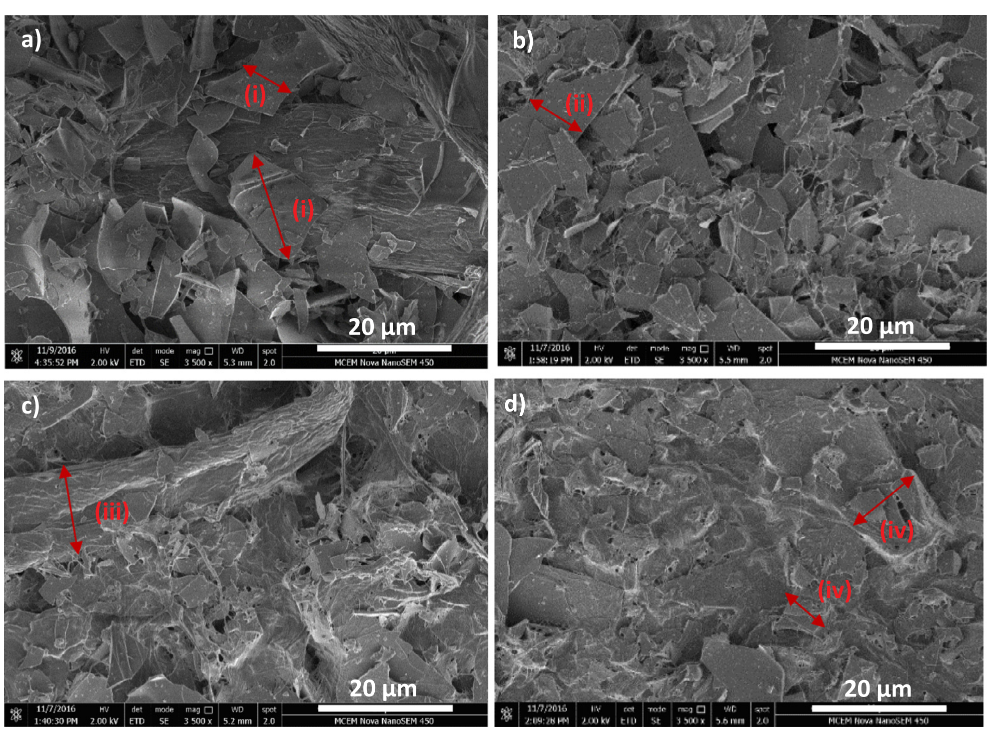

Fig. 5. SEM images of composites: **(a)** Unrefined/Per/PAE, **(b)** Refined/Per/PAE, **(c)** Homogenized(1pass)/Per/PAE and **(d)** Homogenized(3pass)/Per/PAE.

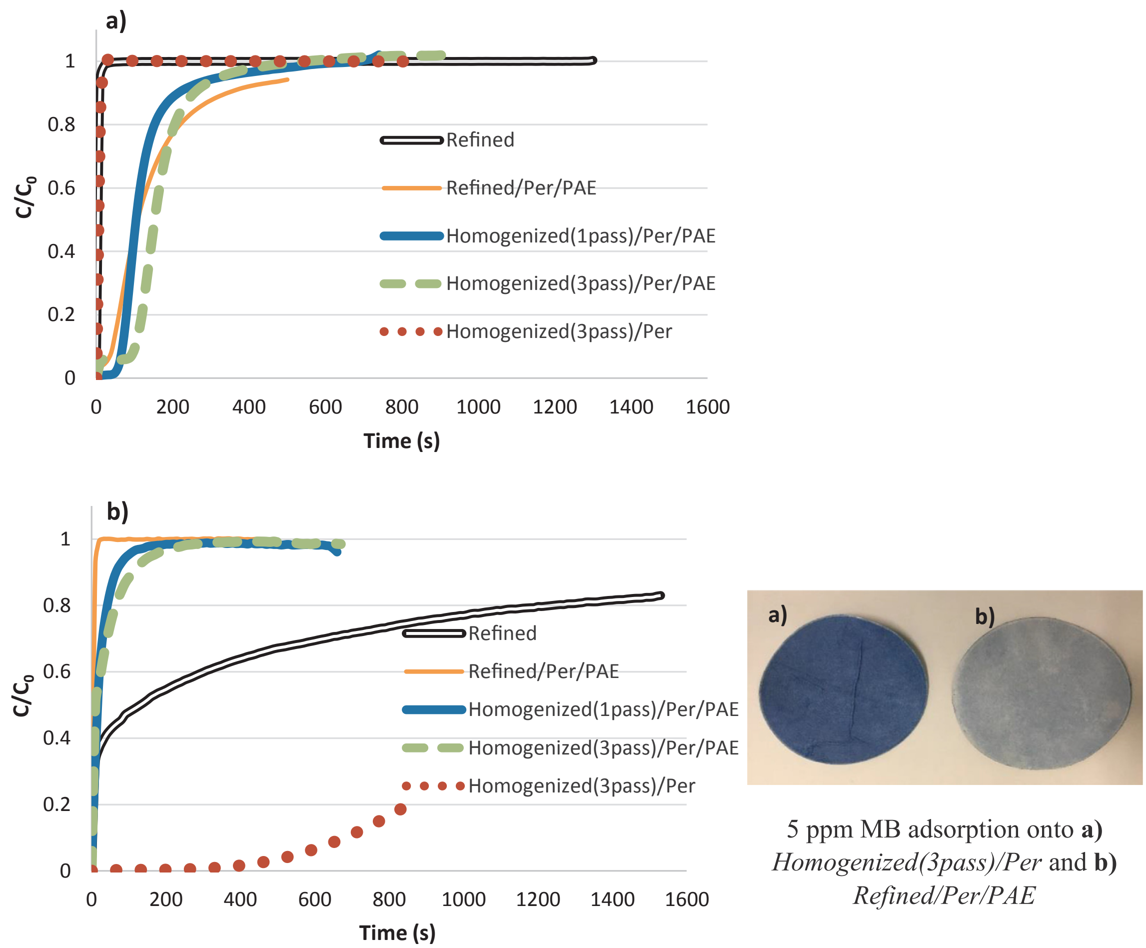

Fig. 6. Adsorption breakthrough curves for **(a)** Metanil yellow and **(b)** Methylene blue at 1.5 bar for filters of different charges and extent of mechanical treatment.

94% MB removal was achieved with composites made with highly fibrillated cellulose but without PAE (*Homogenized(3pass)/Per*); the maximum removal of MY was around 28% for the composites with refined fibres and PAE (*Refined/Per/PAE*). Flux remained identical for both dyes for all composites. Flux remarkably decreases with addition of homogenized pulps. The flow rates for each sample and both dyes are reported in SI (Fig. S3a–d).

3.2.2. Filtration

The rejection rate of suspensions with 1 µm SiO_2 particles was determined for the four different filters at an inlet pressure of 1.5 bar. 1 µm particles were selected as model bacteria (1 µm and bigger) to be removed from food streams such as beer, wine or juice [27]. The effect of homogenization, filter medium charge, inlet pressure and suspension pH on filtration performance was measured. The rejection rate and flux are presented at pHs of 5.8 and 7.2 in Fig. 8. The effect of pH was tested as it is an important variable in applications such as food and pharmaceutical; pH can affect cellulosic fibre pore structure and porosity through swelling and modifying bond strength. Filters have more than 90% particle rejection rate at both pH; pH had no effect on rejection. Charge of filter medium and inlet pressure also did not affect filtration efficiency. Rejection is around 99% for the negatively charged cellulose composites made with homogenized fibres (3 pass) (*Homogenized (3pass)/Per)*. The same rejection rate of around 99% was measured for the composites treated with PAE (*Homogenized(3pass)/Per/PAE*) at 2 different pressures (1 and 2 bar) (Fig. 8a).

(Fig. 8b) Flux decreased remarkably after only 1/3 of the fibre fraction substituted with homogenized fibres. Filtration flux decreased by 30–70% compared to dye solution adsorption flux.

4. Discussion

The adsorption of dye onto the perlite-cellulose composites is electrostatically controlled. The major effect of homogenization on adsorption is to increase surface area which also increases the surface and density of accessible charges. An increase in negatively charged sites contributes either to stronger repulsive or attractive forces between filter medium and dye depending on the system. The effect of surface area is revealed by the breakthrough curves of composites made with refined and homogenized pulps. Composites with refined pulp (*Refined/Per/PAE*) have less repulsive forces with negatively charged dye (MY, Fig. 6a) and less attractive forces with the cationic dye (MB, Fig. 6b) compared to other PAE treated composites. As homogenization is applied and the extent of homogenization increases, increasing accessible negative charges on surface remarkably changes the adsorption behaviour of dye molecules onto the composites.

Adding the cationic PAE both modifies the filter charge which changes its adsorption capacity and improves the composite wet strength by cross linking cellulose fibres. For the cationic dye (MB), the electrostatic interactions, maximized by the elimination of PAE, yield higher adsorption capacity. In contrast, PAE triggers higher adsorption of anionic dye (MY) onto the composites. The addition of negatively charged perlite particles also changes the adsorption behaviour significantly; this is similar to the effect of mechanical treatment of fibres and cationic polymer. The remarkably improved breakthrough curve of *Homogenized(3pass)/Per* (Fig. 6b) is attributed to perlite acting as an excellent filter aid [30].

Nanocellulose addition, achieved by fiberizing a fraction of cellulose fibres (1/3), did not affect the filtration performance significantly.

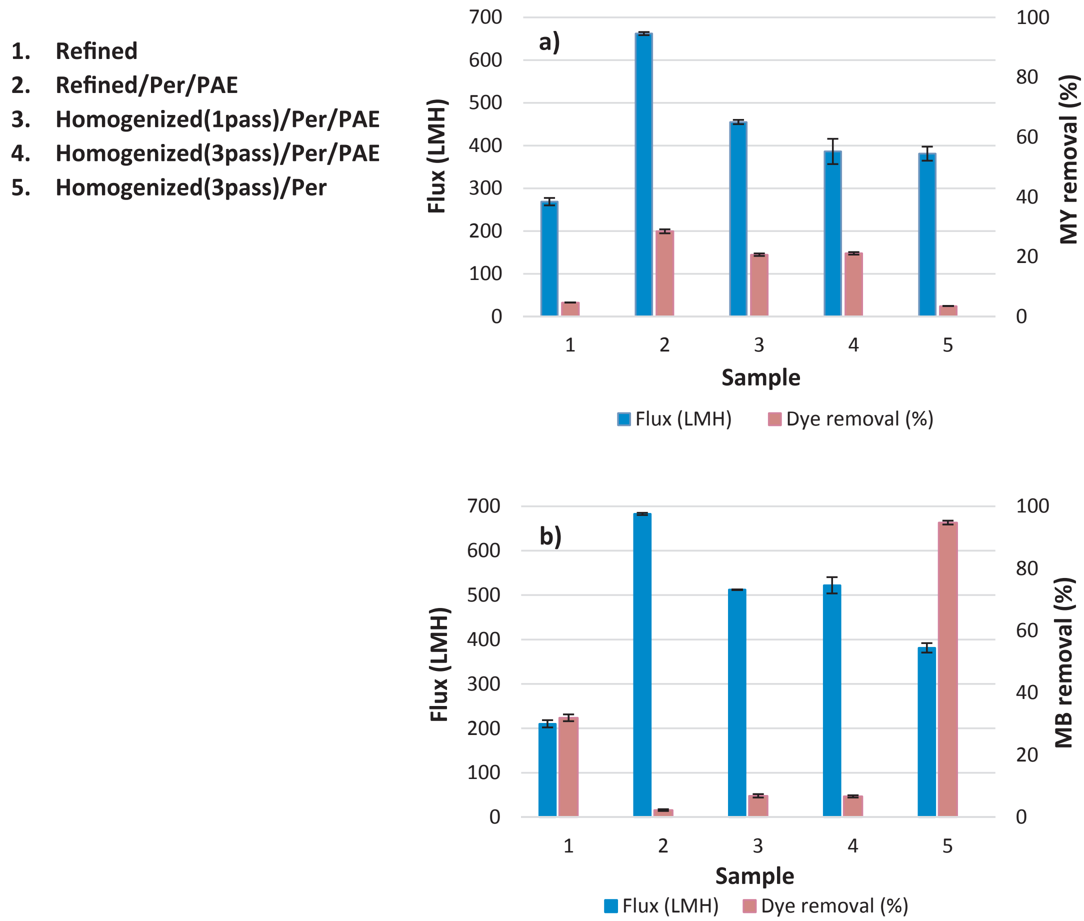

Fig. 7. Flux and total dye removal (%) of samples with **(a)** Metanil yellow and **(b)** Methylene blue dye solutions.

(Fig. 8a). The slight decrease in SiO_2 rejection rate by composites made of highly homogenized fibres (*Homogenized(3pass)/Per/PAE)* at 1.5 bar) is within experimental error. Increasing fibrillation through mechanical treatment intensity did not increase filtration performance.

Homogenization on refined pulp creates a dense and highly fibrillated NC network with a decrease in fibre diameters. The filters made with a small fraction of nano fibres have a more compact and connected structure. The pore size distribution changed remarkably by only substituting 1/3 of the pulp by homogenized fibres. This is due to the web like entangled structure of NC. The more fibrillated the fibres are, the denser the structure is and the less and the smaller are the voids developed between fibres. Composite porosity and pore size distribution can be controlled by modifying fibre diameters. As the homogenization forms smaller pores with denser fibre packing, liquid flux through the composites filters decreases with homogenized pulp addition.

The presence of inorganic particle in the filters also affects porosity and pore size distribution. Pure cellulose sheet has the lowest flux value (Fig. 4a and b). This is due to two phenomena: low porosity as there is no settlement of particles between fibres; decreasing flow rate in time as the fibres compress under pressure (Fig. S3a–d). This compressibility of fibres is well known [31] and leads to poor flux. High loading of inorganic particles prevents this compression so the composites retain high flow rates with very slight change over time.

There is only a weak relation between flux and dye removal capacity – as measured with both dyes (Fig. 7). While less adsorption generally occurs at high fluxes, adsorption is mostly affected by the charge of the filter medium and the solute molecules (Fig. 7a), regardless of flux. Similarly, there was no correlation between rejection rate of 1 µm particles and flux. *Homogenized(3pass)/Per/PAE* successfully removed 99% of the particles at both 1 and 2 bar.

The high filtration rejection of 1 µm particles achieved by the nanocellulose/perlite depth composites is important to the pharmaceutical, food and beverage industry. This brings a new perspective in cold pasteurization to remove microorganisms ranging from 1 to 2 µm [26] and remove ionic compounds [32] (acids and phenolic compounds) without heat treatment which affects taste or denaturing active ingredients. The concept is to rely on the inorganic particles for the selective adsorption of organic molecules, PAE treatment for the retention of colloids- based on charge and filtration for the pasteurization. Nanocellulose-inorganic depth composites can easily be engineered for specific liquid stream purification.

5. Conclusion

Cellulose fibre-perlite composites were prepared using a paper making technique for liquid filtration and adsorption applications. Perlite content was maintained at 70 wt% and the fibre composition was varied with partial substitution of pulp homogenized to different intensities; this was to control fibre structure by increased bonding area and decreasing porosity. A well-known wet strength agent, polyamide-amine-epichlorohydrin (PAE), was used for two purposes; first to provide wet strength; second, to control charge and capacity of filter medium. Two oppositely charged dyes were investigated as models to characterize the adsorption behaviour. The adsorption of dye is electrokinetically controlled and selective adsorption can be achieved by engineering the attractive and repulsive forces. The presence of highly fibrillated NC increased the surface area and also the amount of negative charges accessible in the medium. Increase in negatively charged sites contributed to attractive/repulsive forces depending on the type of

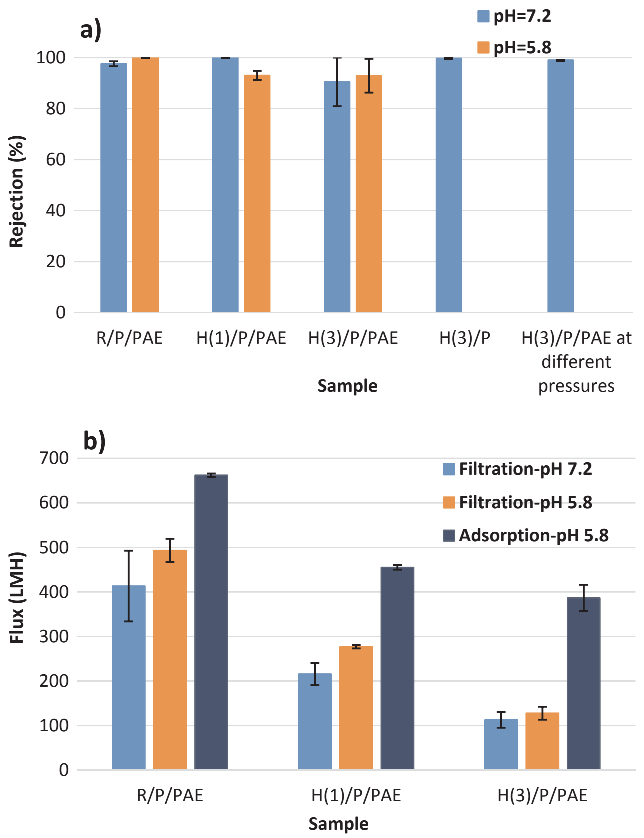

Fig. 8. (a) SiO_2 particle rejection rate (%) of Refined/Per/PAE, Homogenized (1pass)/Per/PAE, Homogenized(3pass)/Per/PAE, Homogenized(3pass)/Per at 1.5 bar and Homogenized (3pass)/Per/PAE at 1 and 2 bar **(b)** Adsorption and filtration flux of Refined/Per/PAE, Homogenized(1pass)/Per/PAE, Homogenized(3pass)/Per/PAE at 1.5 bar.

dye. Homogenized pulp also yielded smaller pore sizes which decreased flux. PAE addition controls and can reverse the charge of filters which substantially affected adsorption performance but it had no effect on filtration efficiency. The composites were efficient in filtration with 90% rejection rate of 1 µm particles. The high filtration capability of the composites at high flux is promising for cold pasteurization in which bacteria (1 µm) are removed at higher than 99% efficiency. Nanocellulose-depth composites provide new purification opportunities in pharmaceutical and food product stream by combining adsorption and filtration to remove interfering elements and colloids.

Acknowledgements

This work was supported by 3M Australia. The authors also acknowledge the Monash Centre for electron microscopy for the facilities used.

Appendix A. Supplementary material

Supplementary data associated with this article can be found, in the online version, at https://doi.org/10.1016/j.seppur.2018.04.038.

References

[1] I.M. Hutten, Chapter 7 - liquid filter applications, Handbook of Nonwoven Filter Media, second ed., Butterworth-Heinemann, Oxford, 2016, pp. 409–450.
[2] M.F. Jimenez-Solomon, P. Gorgojo, M. Munoz-Ibanez, A.G. Livingston, Beneath the surface: influence of supports on thin film composite membranes by interfacial polymerization for organic solvent nanofiltration, J. Membr. Sci. 448 (2013) 102–113.
[3] S. Ramaswamy, A.R. Greenberg, W.B. Krantz, Fabrication of poly (ECTFE) membranes via thermally induced phase separation, J. Membr. Sci. 210 (2002) 175–180.
[4] S. Jiang, Y. Li, B.P. Ladewig, A review of reverse osmosis membrane fouling and control strategies, Sci. Total Environ. 595 (2017) 567–583.
[5] A. Mukhopadhyay, 8 - Composite nonwovens in filters: applications, Composite Non-Woven Materials, Woodhead Publishing, 2014, pp. 164–210.
[6] D. Klemm, F. Kramer, S. Moritz, T. Lindström, M. Ankerfors, D. Gray, A. Dorris, Nanocelluloses: a new family of nature-based materials, Angew. Chem. Int. Ed. 50 (2011) 5438–5466.
[7] R. Andrade, O. Skurtys, F. Osorio, R. Zuluaga, P. Gañán, C. Castro, Wettability of gelatin coating formulations containing cellulose nanofibers on banana and eggplant epicarps, LWT – Food Sci. Technol. 58 (2014) 158–165.
[8] K. Dimic-Misic, C. Ridgway, T. Maloney, J. Paltakari, P. Gane, Influence on pore structure of micro/nanofibrillar cellulose in pigmented coating formulations, Transp. Porous Media 103 (2014) 155–179.
[9] J. Kim, G. Montero, Y. Habibi, J.P. Hinestroza, J. Genzer, D.S. Argyropoulos, O.J. Rojas, Dispersion of cellulose crystallites by nonionic surfactants in a hydrophobic polymer matrix, Polym. Eng. Sci. 49 (2009) 2054–2061.
[10] G. Rodionova, M. Lenes, Ø. Eriksen, Ø. Gregersen, Surface chemical modification of microfibrillated cellulose: improvement of barrier properties for packaging applications, Cellulose 18 (2011) 127–134.
[11] C. Salas, T. Nypelö, C. Rodriguez-Abreu, C. Carrillo, O.J. Rojas, Nanocellulose properties and applications in colloids and interfaces, Curr. Opin. Colloid Interface Sci. 19 (2014) 383–396.
[12] Z. Karim, S. Claudpierre, M. Grahn, K. Oksman, A.P. Mathew, Nanocellulose based functional membranes for water cleaning: tailoring of mechanical properties, porosity and metal ion capture, J. Membr. Sci. 514 (2016) 418–428.
[13] H. Ma, B.S. Hsiao, B. Chu, Ultrafine cellulose nanofibers as efficient adsorbents for removal of UO_2^{2+} in water, ACS Macro Lett. 1 (2012) 213–216.
[14] A. Mautner, K.Y. Lee, P. Lahtinen, M. Hakalahti, T. Tammelin, K. Li, A. Bismarck, Nanopapers for organic solvent nanofiltration, Chem. Commun. 50 (2014) 5778–5781.
[15] A. Mautner, K.-Y. Lee, T. Tammelin, A.P. Mathew, A.J. Nedoma, K. Li, A. Bismarck, Cellulose nanopapers as tight aqueous ultra-filtration membranes, React. Funct. Polym. 86 (2015) 209–214.
[16] H. Sehaqui, A. Mautner, U. Perez de Larraya, N. Pfenninger, P. Tingaut, T. Zimmermann, Cationic cellulose nanofibers from waste pulp residues and their nitrate, fluoride, sulphate and phosphate adsorption properties, Carbohydr. Polym. 135 (2016) 334–340.
[17] H. Sehaqui, B. Michen, E. Marty, L. Schaufelberger, T. Zimmermann, Functional cellulose nanofiber filters with enhanced flux for the removal of humic acid by adsorption, ACS Sustain. Chem. Eng. 4 (2016) 4582–4590.
[18] H. Sehaqui, U. Perez de Larraya, P. Tingaut, T. Zimmermann, Humic acid adsorption onto cationic cellulose nanofibers for bioinspired removal of copper(ii) and a positively charged dye, Soft Matter 11 (2015) 5294–5300.
[19] S. Srivastava, A. Kardam, K.R. Raj, Nanotech reinforcement onto cellulosic fibers: green remediation of toxic metals, Int. J. Green Nanotechnol. 4 (2012) 46–53.
[20] X. Yu, S. Tong, M. Ge, L. Wu, J. Zuo, C. Cao, W. Song, Adsorption of heavy metal ions from aqueous solution by carboxylated cellulose nanocrystals, J. Environ. Sci. 25 (2013) 933–943.
[21] J.J. Blaker, K.-Y. Lee, A. Bismarck, Hierarchical composites made entirely from renewable resources, J. Biobased Mater. Bioenergy 5 (2011) 1–16.
[22] N. Keshavarzi, F. Mashayekhy Rad, A. Mace, F. Ansari, F. Akhtar, U. Nilsson, L. Berglund, L. Bergström, Nanocellulose-zeolite composite films for odor elimination, ACS Appl. Mater. Interfaces 7 (2015) 14254–14262.
[23] S. Varanasi, Z.-X. Low, W. Batchelor, Cellulose nanofibre composite membranes – biodegradable and recyclable UF membranes, Chem. Eng. J. 265 (2015) 138–146.
[24] Z. Karim, A.P. Mathew, V. Kokol, J. Wei, M. Grahn, High-flux affinity membranes based on cellulose nanocomposites for removal of heavy metal ions from industrial effluents, RSC Adv. 6 (2016) 20644–20653.
[25] G.J. Freeman, 11 - Reducing microbial spoilage of beer using filtration A2, in: Annie E. Hill (Ed.), Brewing Microbiology, Woodhead Publishing, Oxford, 2015, pp. 241–251.
[26] V. Millet, A. Lonvaud-Funel, The viable but non-culturable state of wine microorganisms during storage, Lett. Appl. Microbiol. 30 (2000) 136–141.
[27] C. Peri, M. Riva, P. Decio, Crossflow membrane filtration of wines: comparison of performance of ultrafiltration, microfiltration, and intermediate cut-off membranes, Am. J. Enol. Viticult. 39 (1988) 162–168.
[28] T.M. Toland, K.C. Fugelsang, C.J. Muller, Methods for estimating protein instability in white wines: a comparison, Am. J. Enol. Viticult. 47 (1996) 111–112.
[29] H. Giesche, Mercury porosimetry: a general (practical) overview, Part. Part. Syst. Char. 23 (2006) 9–19.
[30] M. Doğan, M. Alkan, Y. Onganer, Adsorption of methylene blue from aqueous solution onto perlite, Water Air Soil Pollut. 120 (2000) 229–248.
[31] P. Orsolini, B. Michen, A. Huch, P. Tingaut, W.R. Caseri, T. Zimmermann, Characterization of pores in dense nanopapers and nanofibrillated cellulose membranes: a critical assessment of established methods, ACS Appl. Mater. Interfaces 7 (2015) 25884–25897.
[32] J.A. Considine, E. Frankish, Chapter 3 – wine chemistry, A Complete Guide to Quality in Small-Scale Wine Making, Academic Press, San Diego, 2014, pp. 23–50.